This copy of the ESI replaces the previous version published on 21 Feb 2022

SUPPORTING INFORMATION

BENCHMARKS OF THE DENSITY FUNCTIONAL TIGHT-BINDING METHOD FOR REDOX, PROTONATION AND ELECTRONIC PROPERTIES OF QUINONES

Maureen M. Kitheka,[a] Morgan Redington,[a] Jibo Zhang,[b] Yan Yao,[b] Puja Goyal[a]*

[a]Department of Chemistry, State University of New York at Binghamton, Binghamton, NY 13905, USA
[b]Department of Electrical and Computer Engineering and Texas Center for Superconductivity at the University of Houston, Houston, Texas 77024, USA

TABLE OF CONTENTS

Page

1. Effect of solvent model on DFT reduction potentials

The conductor-like polarizable continuum model (CPCM) and the integral equation formalism polarizable continuum model (IEFPCM) yield very similar reduction potential values as shown in **Table S1**.

Table S1 Effect of implicit solvent model on the reduction potential (V) of selected quinones calculated with B3LYP/6-31++G**

Molecule	CPCM	IEFPCM
Phenanthrenequinone (PQ)	-0.218	-0.221
Pyrene-4,5-dione (PDO)	-0.228	-0.219
Pyrene-4,5,9,10-tetrone (PTO)	0.0214	0.0741

2. Effect of implicit vs. explicit water on DFTB3 reduction potentials

Table S2 Effect of solvent description on the reduction potential (V) of selected quinones calculated using DFTB3/3OB

Method	2-methoxybenzoquinone (MBQ)	1,4-napthoquinone (1,4-NQ)
DFTB3/3OB Implicit[a]	-0.114	-0.188
DFTB3/3OB Explicit MM[b]	-0.145	-0.271
DFTB3/3OB Implicit/Few Explicit QM[c]	-0.108	-0.200

[a]Implicit water described using the conductor-like screening model (COSMO)
[b]Explicit water described using the modified TIP3P water model and periodic boundary conditions
[c]Two water molecules hydrogen bonded to each carbonyl group treated quantum mechanically (QM) with DFTB3/3OB; quinone and explicit water immersed in implicit water described using COSMO

3. Effect of dispersion on reduction potentials

Table S3 Effect of dispersion on the reduction potential (V) of selected quinones.

Quinone	B3LYP/ 6-31++G**, CPCM	B3LYP-D3/ 6-31++G**, CPCM	DFTB3/3OB, Implicit[a]	DFTB3-D3/3OB, Implicit[a]	DFTB3/3OB, Implicit/Few Explicit QM[b]	DFTB3-D3/3OB, Implicit/Few Explicit QM[b]
MBQ	-0.039	-	-0.114	-0.114	-0.108	-0.083
1,4-NQ	-0.175	-0.176	-0.188	-0.187	-0.200	-0.195
PQ	-0.218	-	-0.265	-0.264	-	-
PDO	-0.228	-	-0.305	-0.305	-	-
PTO	0.021	-	0.123	0.123	-	-

[a]Implicit water described using the conductor-like screening model (COSMO)
[b]Two water molecules hydrogen bonded to each carbonyl group treated quantum mechanically with DFTB3/3OB; quinone and explicit water immersed in implicit water described using COSMO

4. Simulation Procedure for Thermodynamic Integration (TI) Calculations

In all minimization, equilibration and production runs in the thermodynamic integration calculations, the non-bonded cutoff distance was 12.0 Å. The cutoff radius used for generating the non-bonded pair list was 14 Å and this list was updated heuristically. The particle mesh Ewald method[1] was used to treat long range electrostatics. Lennard-Jones interactions were calculated

using the shift method. Energy minimization was carried out in two stages, using the steepest descent algorithm for 1000 steps followed by the adopted basis Newton-Raphson algorithm[2] with a gradient tolerance of 0.1 kcal mol^{-1} $Å^{-1}$. This was followed by 50 ps of heating and equilibration at 300K using the Leapfrog integrator[3] and a timestep of 1 fs. During heating/equilibration and the subsequent production runs, the SHAKE algorithm[4] was used to apply constraints on all bonds involving hydrogen atoms and a harmonic restraint with a force constant of 2.0 kcal mol^{-1} $Å^{-1}$ was applied to restrain the center of mass of the solute to the origin. Production simulations were carried out for 400 ps for all the λ windows using the velocity Verlet algorithm with the Nosé-Hoover thermostat to maintain the temperature at 300 K.

5. Time Evolution of the Energy Gap in TI calculations

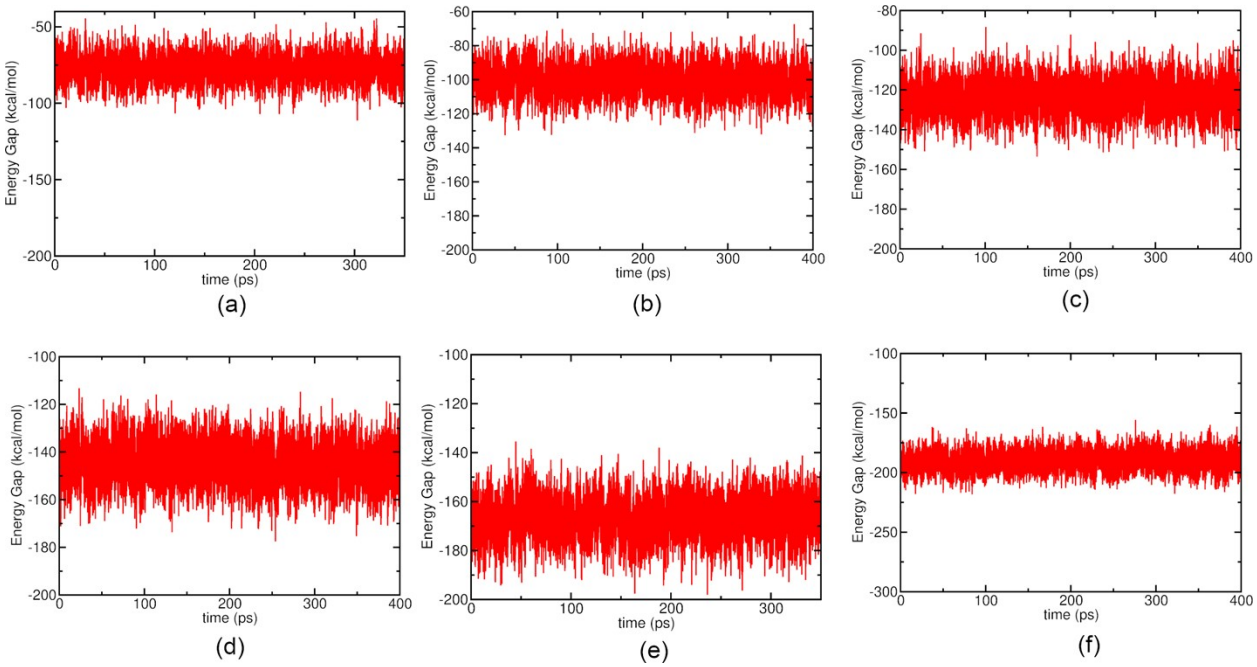

Fig. S1 Time evolution of the energy gap in production simulations for different λ windows in TI calculations of the reduction potential of 1,4-benzonquinone (BQ) in water. (a) λ=0.0, (b) λ=0.2, (c) λ=0.4, (d) λ=0.6, (e) λ=0.8, and (f) λ=1.0. Only time segments with equilibrated average energy gap are shown.

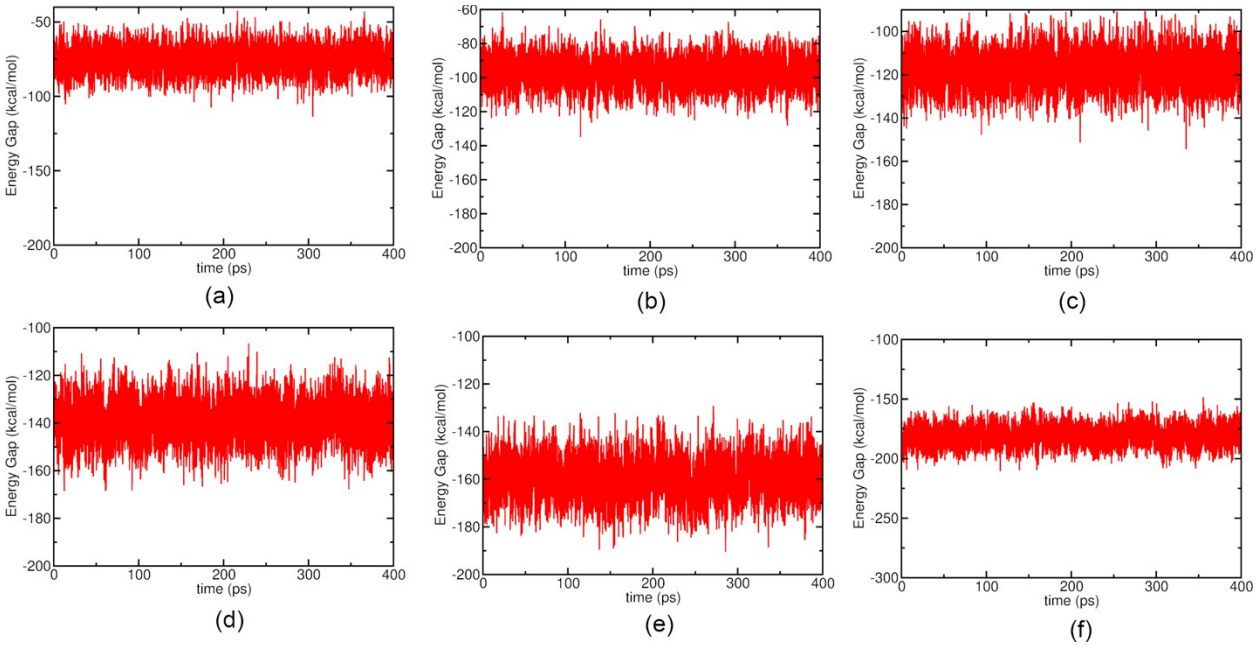

Fig. S2 Time evolution of the energy gap in production simulations for different λ windows in TI calculations of the reduction potential of 2-methoxybenzoquinone (MBQ) in water. (a) λ=0.0, (b) λ=0.2, (c) λ=0.4, (d) λ=0.6, (e) λ=0.8, and (f) λ=1.0. Only time segments with equilibrated average energy gap are shown.

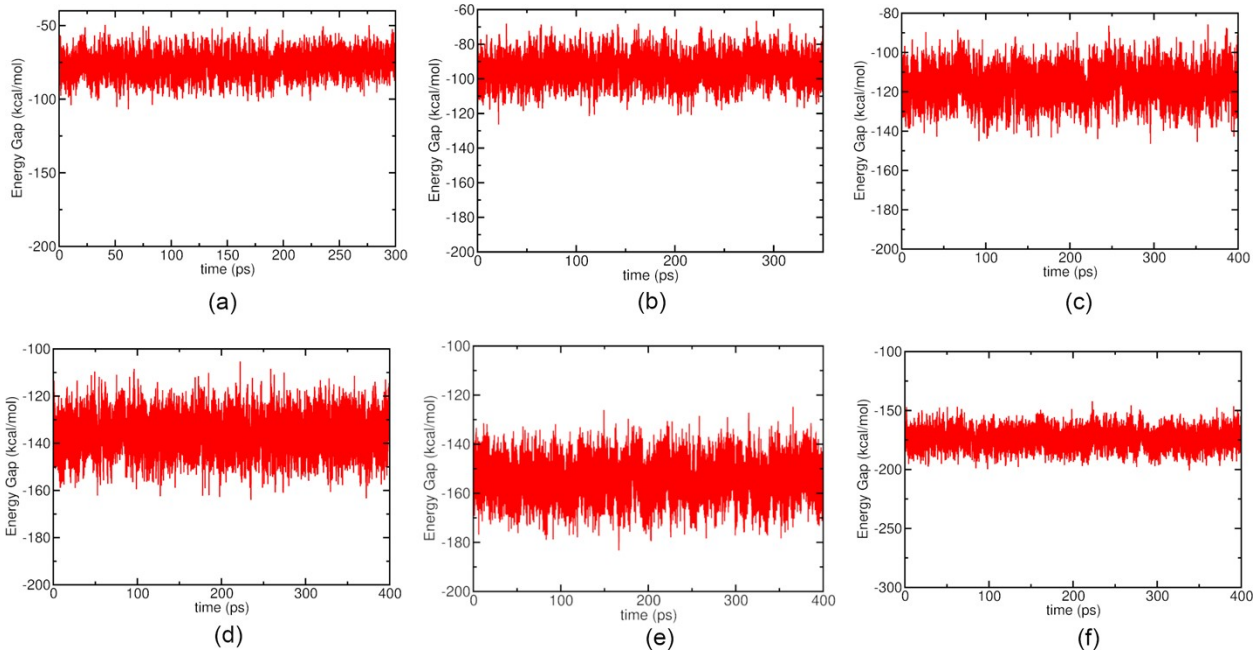

Fig. S3 Time evolution of the energy gap in production simulations for different λ windows in TI calculations of the reduction potential of 1,4-napthoquinone (1,4-NQ) in water. (a) λ=0.0, (b) λ=0.2, (c) λ=0.4, (d) λ=0.6, (e) λ=0.8, and (f) λ=1.0. Only time segments with equilibrated average energy gap are shown.

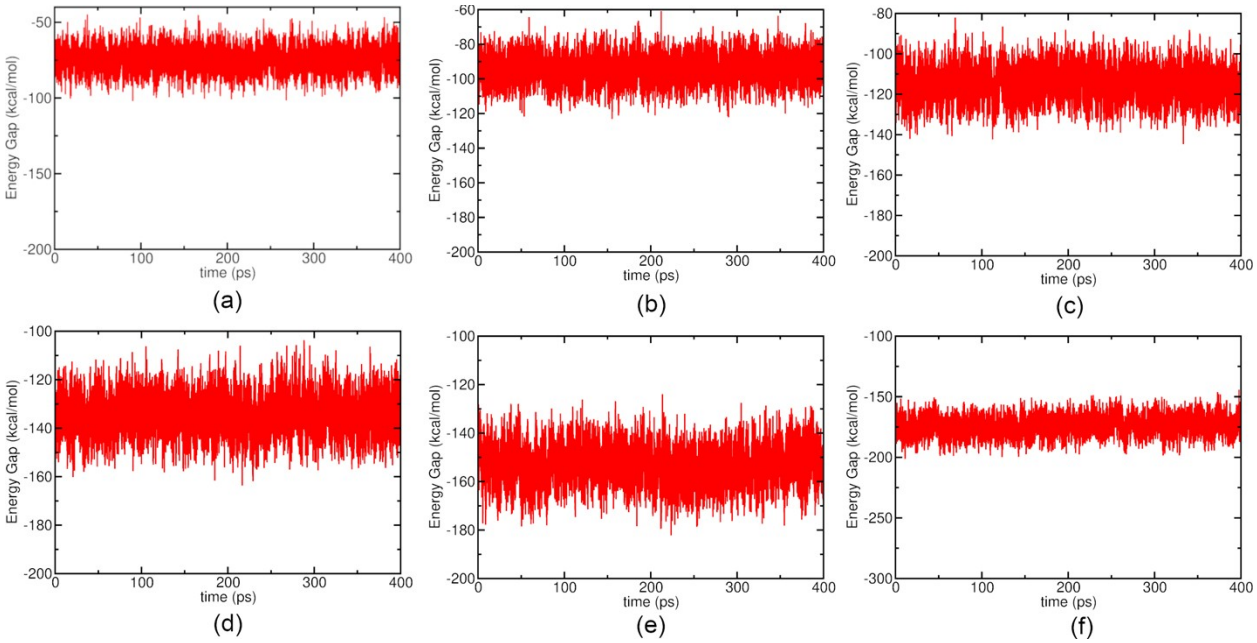

Fig. S4 Time evolution of the energy gap in production simulations for different λ windows in TI calculations of the reduction potential of 1,2-napthoquinone (1,2-NQ) in water. (a) λ=0.0, (b) λ=0.2, (c) λ=0.4, (d) λ=0.6, (e) λ=0.8, and (f) λ=1.0. Only time segments with equilibrated average energy gap are shown.

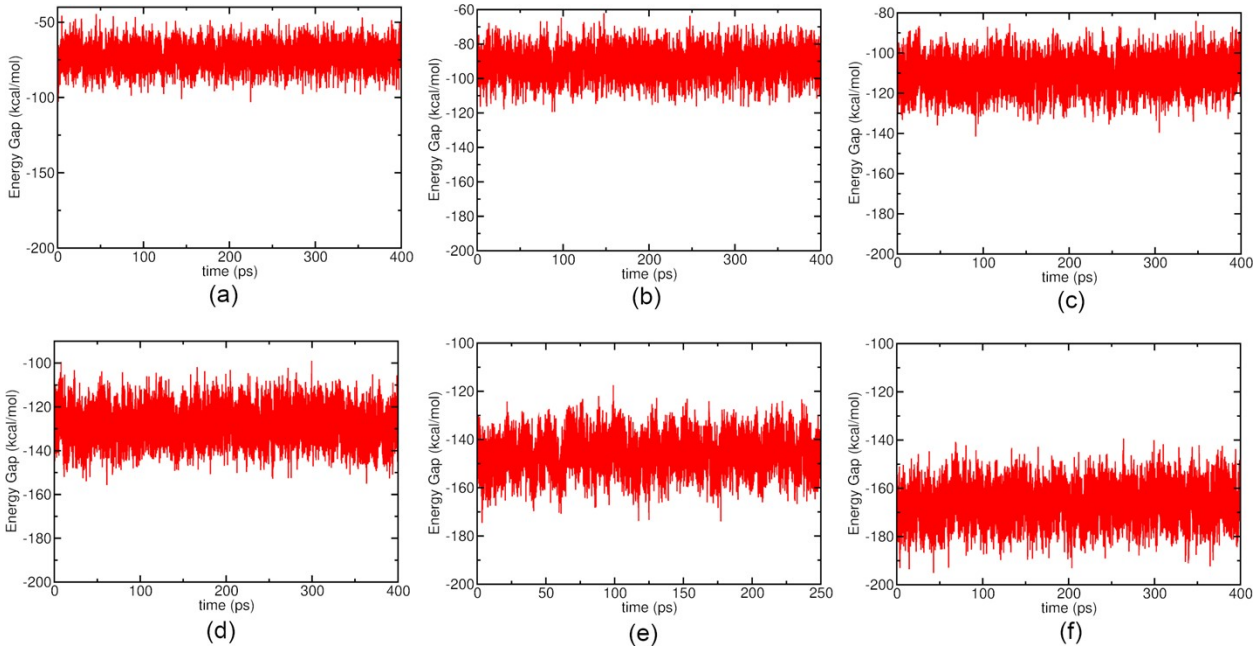

Fig. S5 Time evolution of the energy gap in production simulations for different λ windows in TI calculations of the reduction potential of phenanthrenequinone (PAQ) in water. (a) λ=0.0, (b) λ=0.2, (c) λ=0.4, (d) λ=0.6, (e) λ=0.8, and (f) λ=1.0. Only time segments with equilibrated average energy gap are shown.

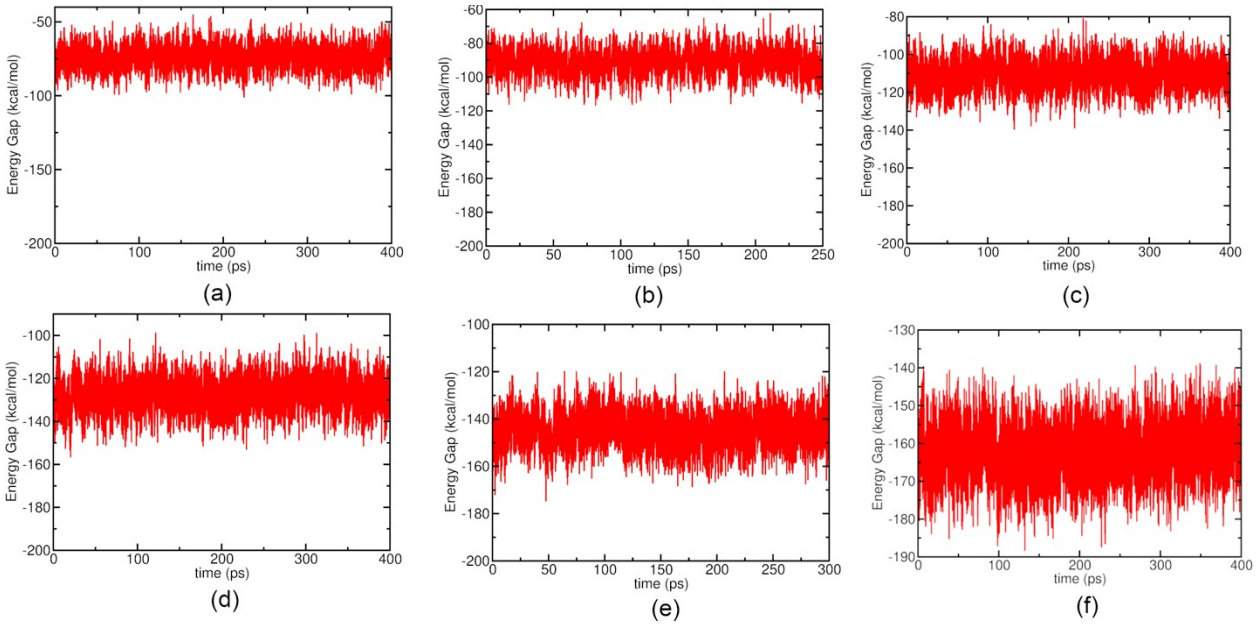

Fig. S6 Time evolution of the energy gap in production simulations for different λ windows in TI calculations of the reduction potential of pyrene-4,5-dione (PDO) in water. (a) λ=0.0, (b) λ=0.2, (c) λ=0.4, (d) λ=0.6, (e) λ=0.8, and (f) λ=1.0. Only time segments with equilibrated average energy gap are shown.

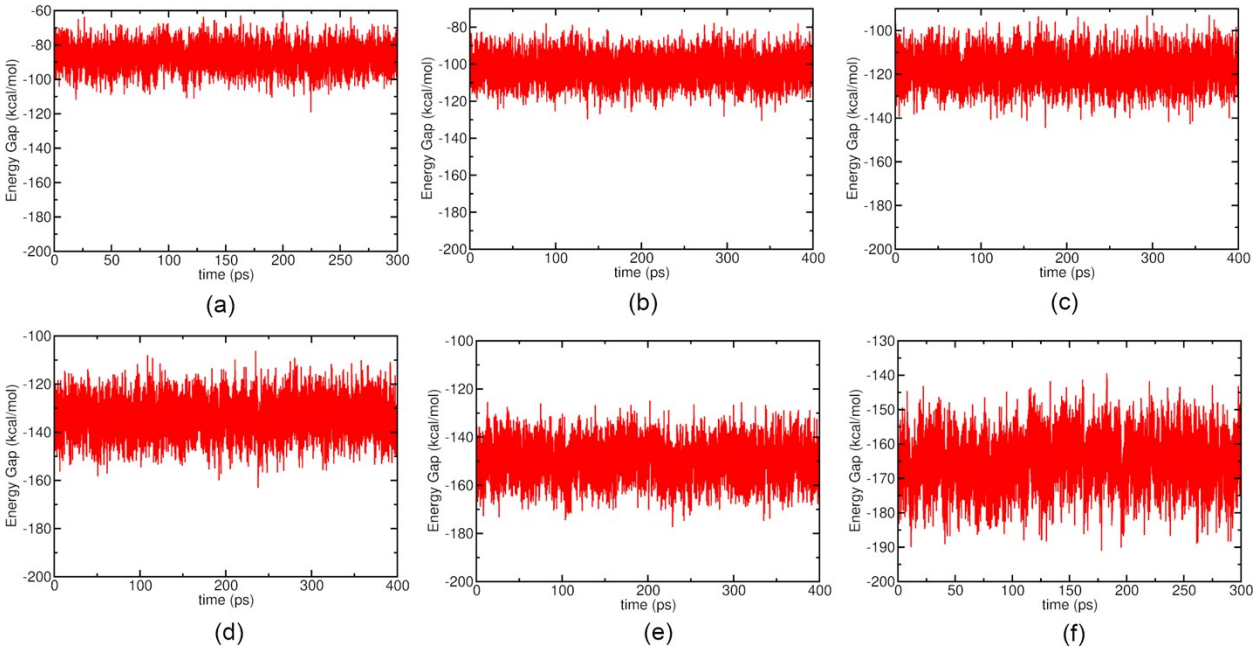

Fig. S7 Time evolution of the energy gap in production simulations for different λ windows in TI calculations of the reduction potential of pyrene-4,5,9,10-tetrone (PTO) in water. (a) λ=0.0, (b) λ=0.2, (c) λ=0.4, (d) λ=0.6, (e) λ=0.8, and (f) λ=1.0. Only time segments with equilibrated average energy gap are shown.

6. Block Averaging

We used the block averaging method to estimate the standard error in the average energy gap for each λ window. This was done by dividing the energy gap data for each λ window into blocks, computing the average from each block, followed by calculation of the standard deviation of the averages and lastly, the standard error. Figs. S8-S14 show that as the block size increases and the data in different blocks becomes more uncorrelated, the standard error increases and finally plateaus.[5,6] We used Eq. S1 to fit the data.

$$y = \frac{a_0}{\left(1 + e^{-a_1 x}\right)} \qquad \text{Eq. S1}$$

Most of the R^2 values were close to 0.97-0.98 and the standard errors were ~0.25-0.30 kcal/mol (judged from the plateau regions of the fitted curves). Some plots show a poor fit to Eq. S1 at small block size values. Larger deviation from the fitted curve is observed at large block size values because the number of blocks (number of data points for which the standard error is computed) is low. Data at very large block sizes is therefore not meaningful and not shown.

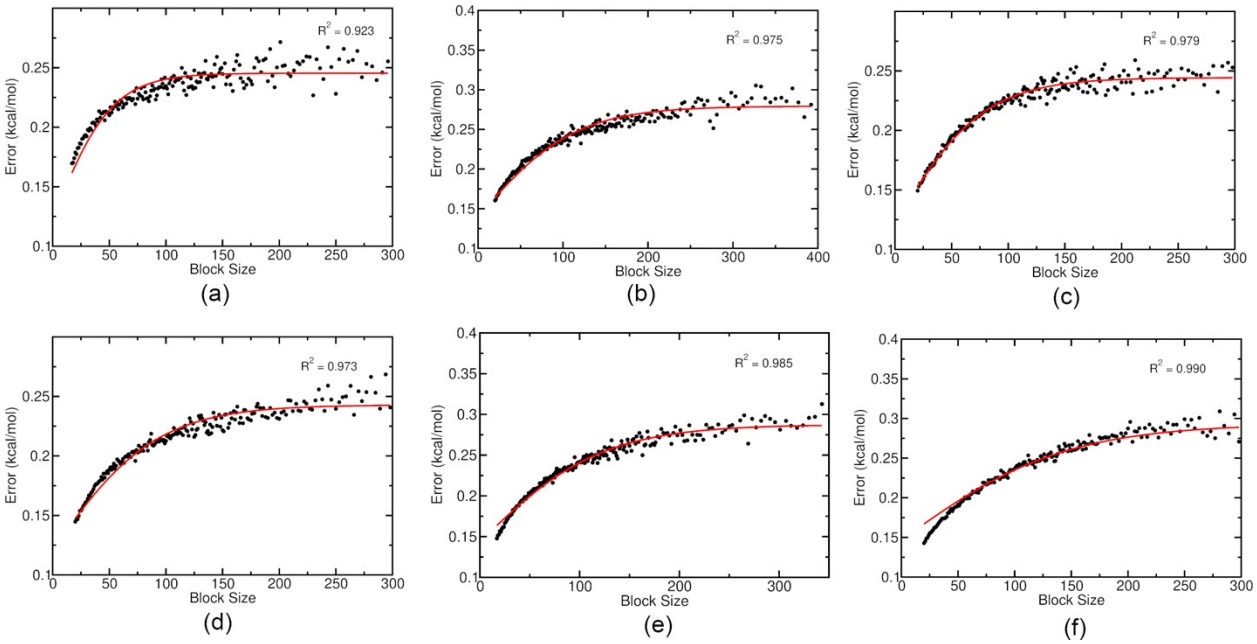

Fig. S8 Standard error of the average energy gap in production simulations for different λ windows in TI calculations of the reduction potential of BQ in water. (a) λ=0.0, (b) λ=0.2, (c) λ=0.4, (d) λ=0.6, (e) λ=0.8, and (f) λ=1.0. The solid curve represents the sigmoidal fit (Eq. S1) and the block size indicates the number of data points in each block. The gap between two consecutive data points corresponds to a time interval of 20 fs.

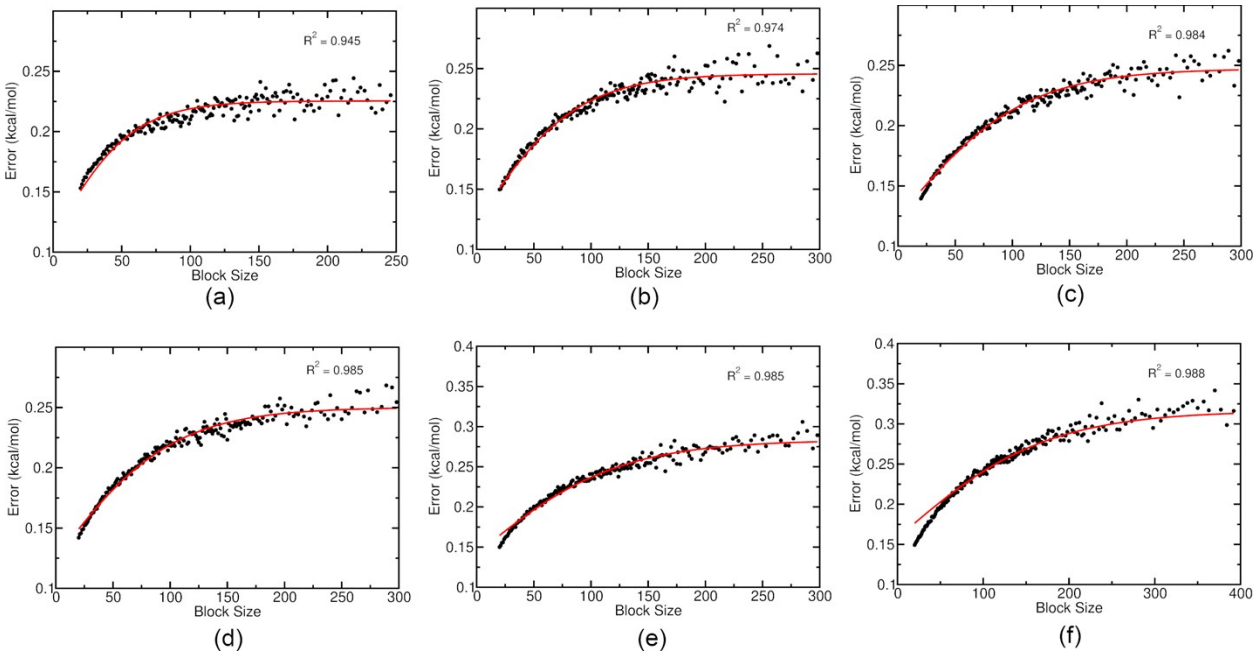

Fig. S9 Standard error of the average energy gap in production simulations for different λ windows in TI calculations of the reduction potential of MBQ in water. (a) λ=0.0, (b) λ=0.2, (c) λ=0.4, (d) λ=0.6, (e) λ=0.8, and (f) λ=1.0. The solid curve represents the sigmoidal fit (Eq. S1) and the block size indicates the number of data points in each block. The gap between two consecutive data points corresponds to a time interval of 20 fs.

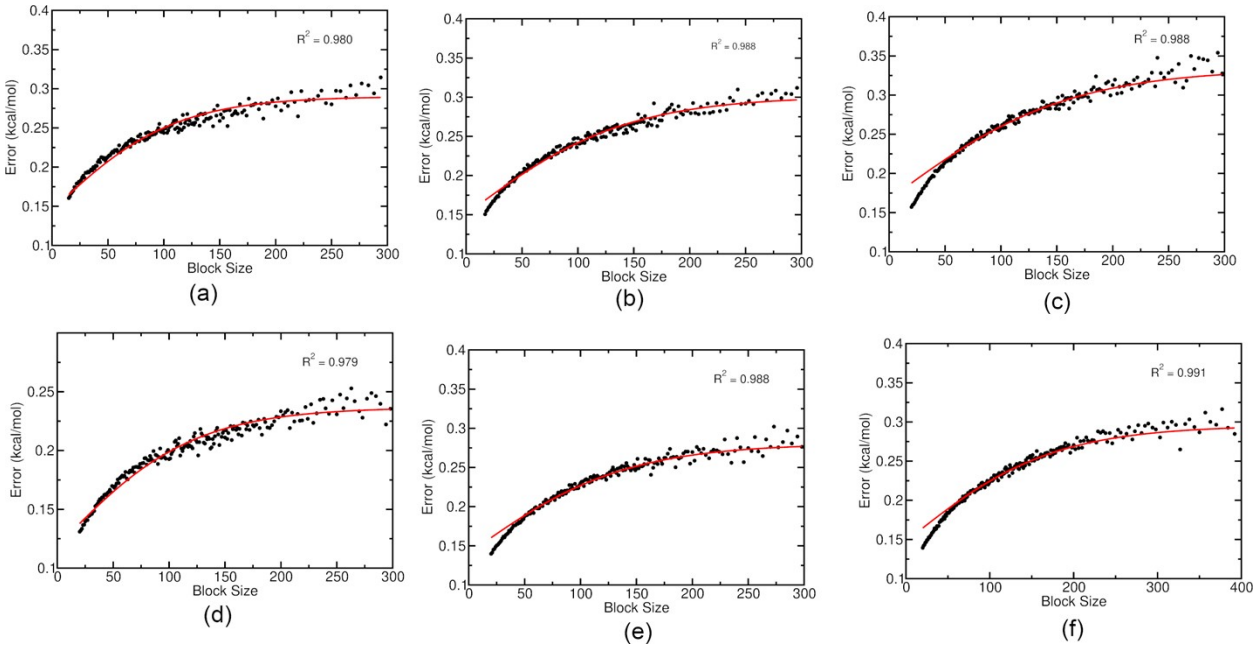

Fig. S10 Standard error of the average energy gap in production simulations for different λ windows in TI calculations of the reduction potential of 1,4-NQ in water. (a) λ=0.0, (b) λ=0.2, (c) λ=0.4, (d) λ=0.6, (e) λ=0.8, and (f) λ=1.0. The solid curve represents the sigmoidal fit (Eq. S1) and the block size indicates the number of data points in each block. The gap between two consecutive data points corresponds to a time interval of 20 fs.

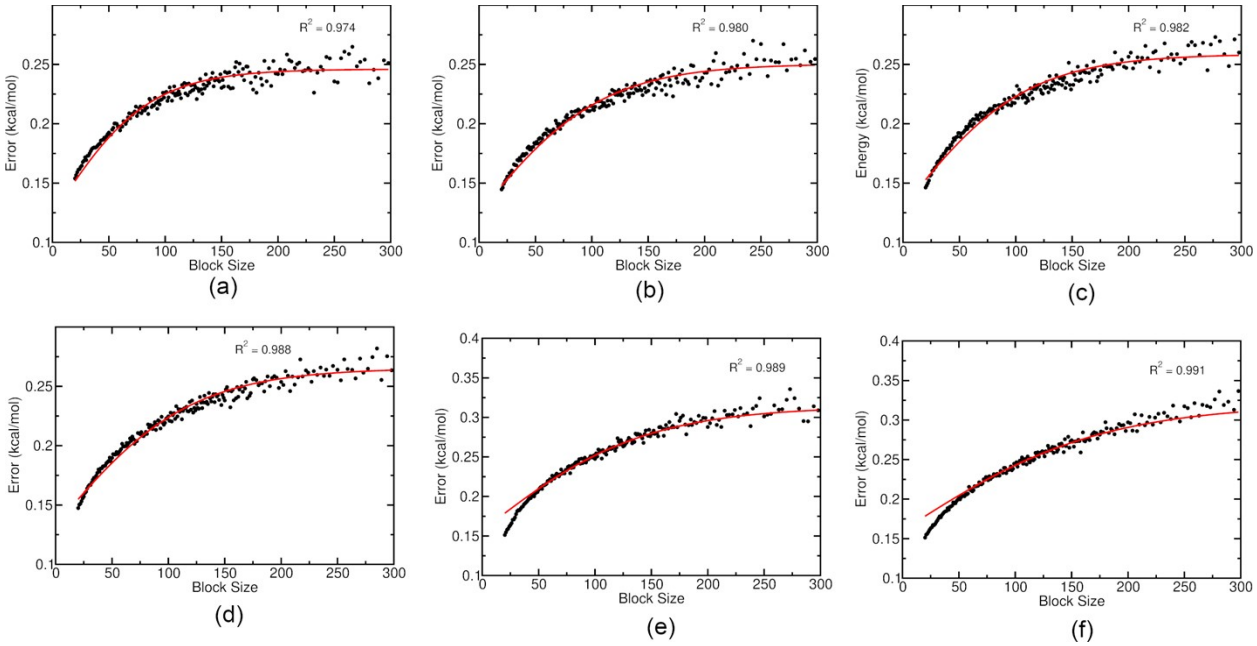

Fig. S11 Standard error of the average energy gap in production simulations for different λ windows in TI calculations of the reduction potential of 1,2-NQ in water. (a) λ=0.0, (b) λ=0.2, (c) λ=0.4, (d) λ=0.6, (e) λ=0.8, and (f) λ=1.0. The solid curve represents the sigmoidal fit (Eq. S1) and the block size indicates the number of data points in each block. The gap between two consecutive data points corresponds to a time interval of 20 fs.

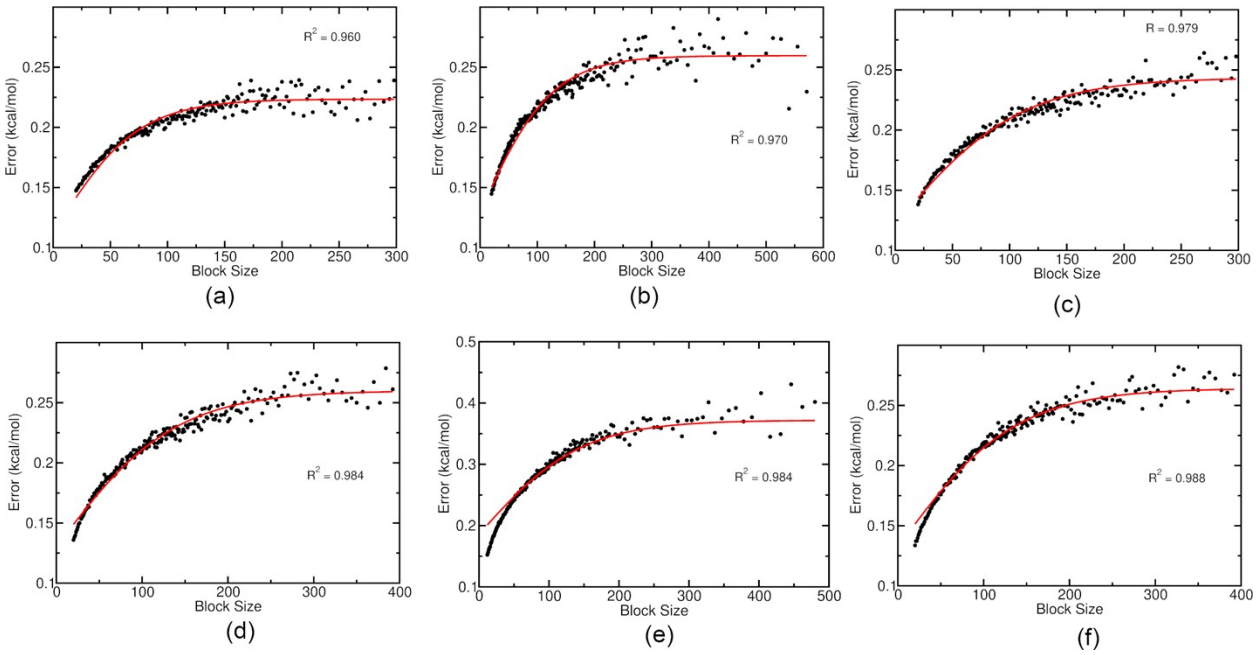

Fig. S12 Standard error of the average energy gap in production simulations for different λ windows in TI calculations of the reduction potential of PAQ in water. (a) λ=0.0, (b) λ=0.2, (c) λ=0.4, (d) λ=0.6, (e) λ=0.8, and (f) λ=1.0. The solid curve represents the sigmoidal fit (Eq. S1) and the block size indicates the number of data points in each block. The gap between two consecutive data points corresponds to a time interval of 20 fs.

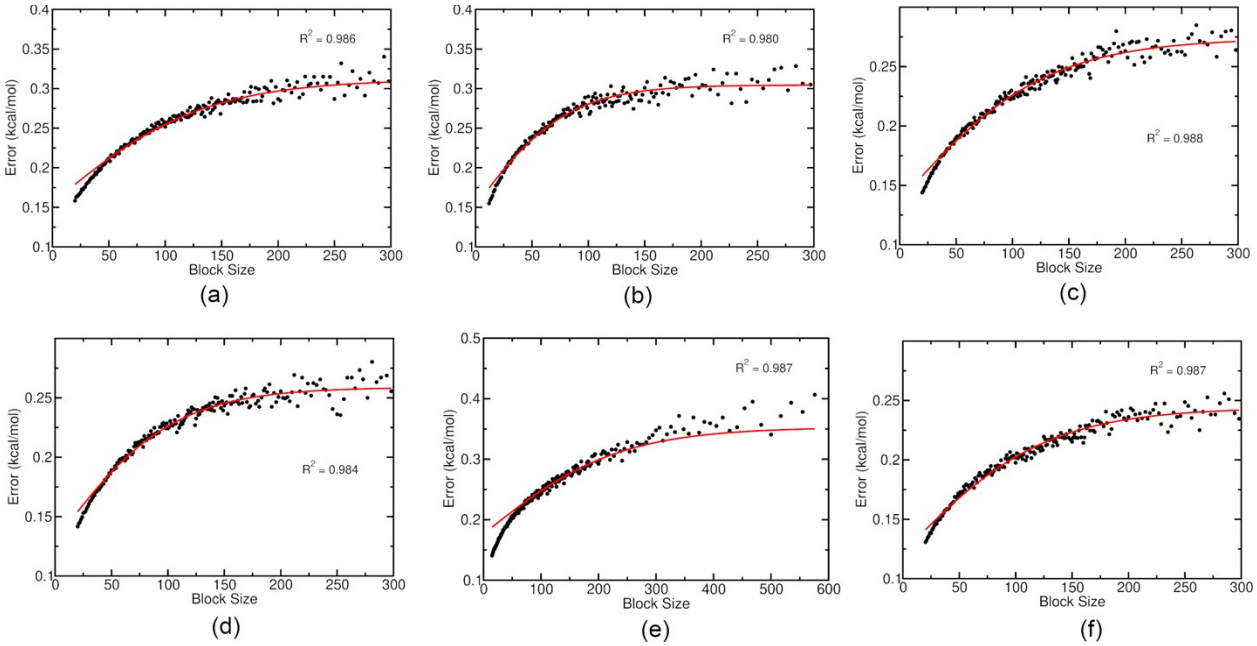

Fig. S13 Standard error of the average energy gap in production simulations for different λ windows in TI calculations of the reduction potential of PDO in water. (a) λ=0.0, (b) λ=0.2, (c) λ=0.4, (d) λ=0.6, (e) λ=0.8, and (f) λ=1.0. The solid curve represents the sigmoidal fit (Eq. S1) and the block size indicates the number of data points in each block. The gap between two consecutive data points corresponds to a time interval of 20 fs.

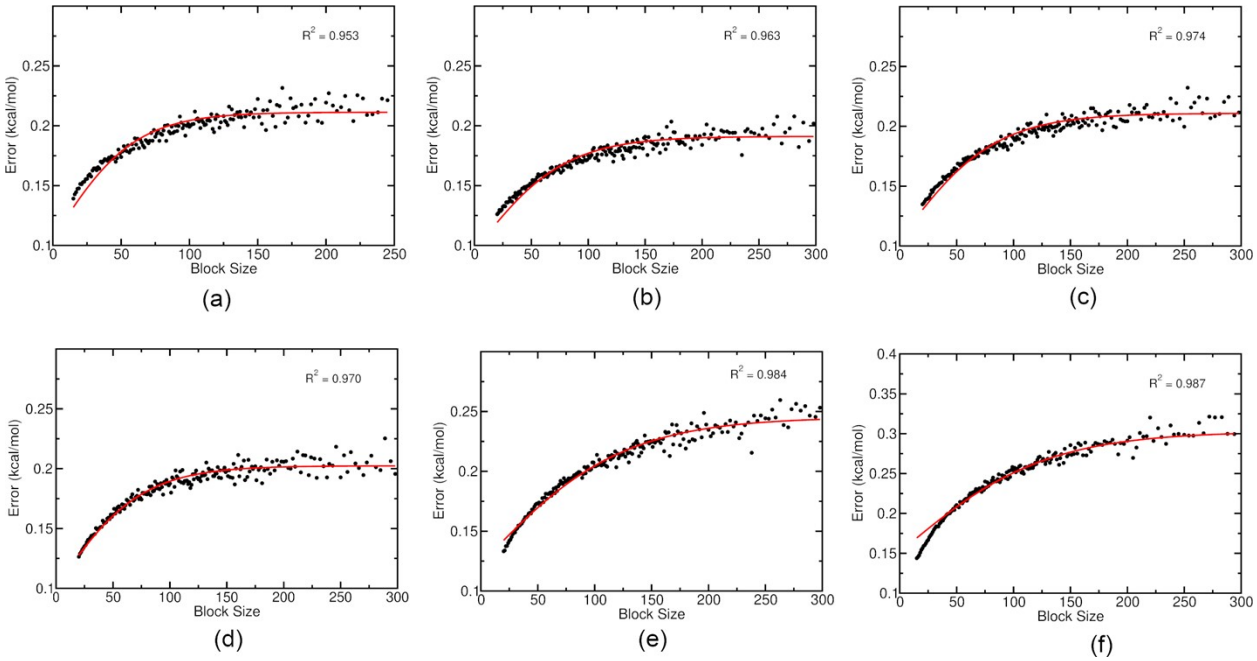

Fig. S14 Standard error of the average energy gap in production simulations for different λ windows in TI calculations of the reduction potential of PTO in water. (a) λ=0.0, (b) λ=0.2, (c) λ=0.4, (d) λ=0.6, (e) λ=0.8, and (f) λ=1.0. The solid curve represents the sigmoidal fit (Eq. S1) and the block size indicates the number of data points in each block. The gap between two consecutive data points corresponds to a time interval of 20 fs.

7. Average Energy Gap as a Function of λ

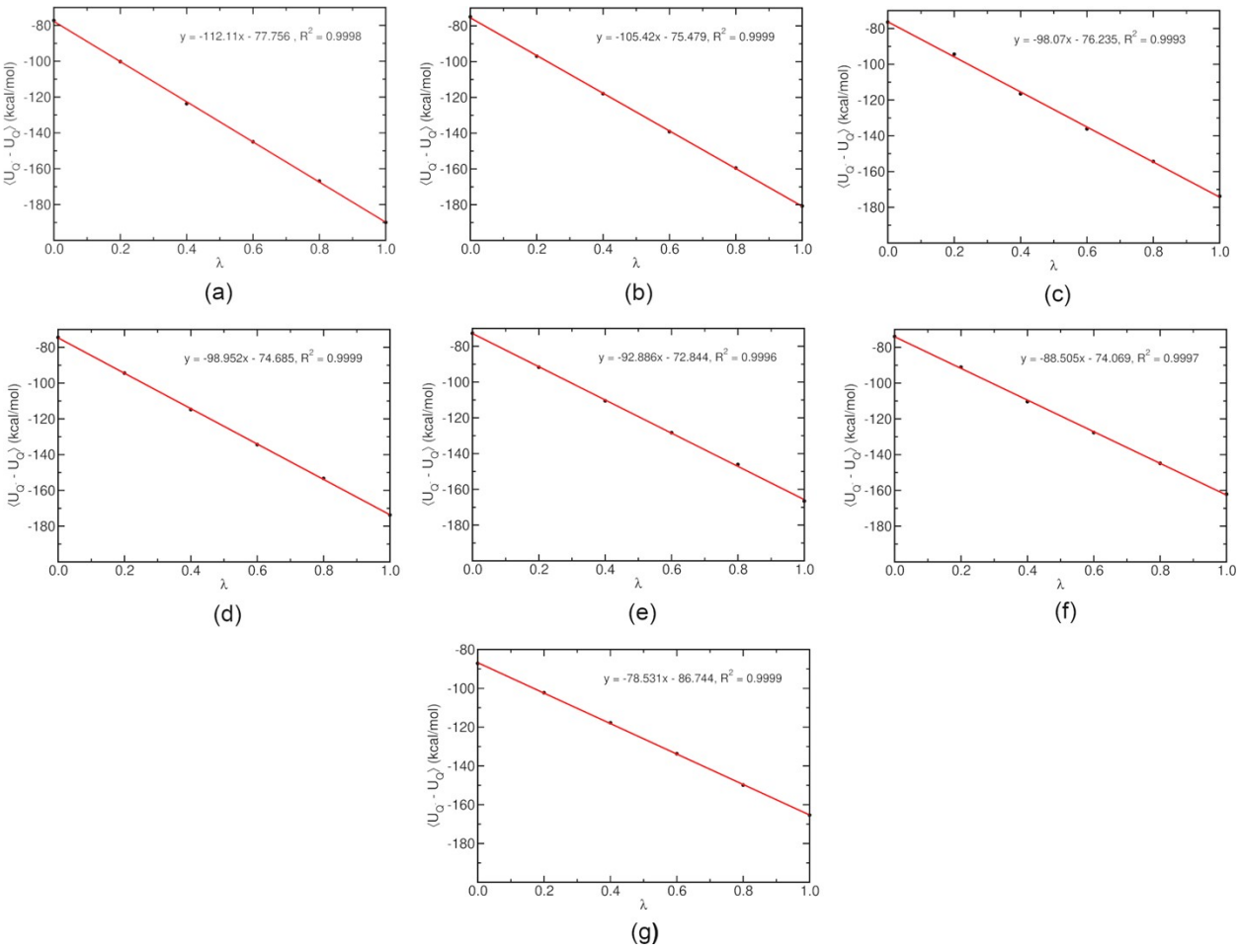

Fig. S15 Average energy gap as a function of λ for (a) BQ, (b) MBQ, (c) 1,4-NQ, (d) 1,2-NQ, (e) PAQ, (f) PDO and (g) PTO. The equation of the linear fit and the corresponding R^2 value are shown in each panel.

8. Proton Transfer Calculations

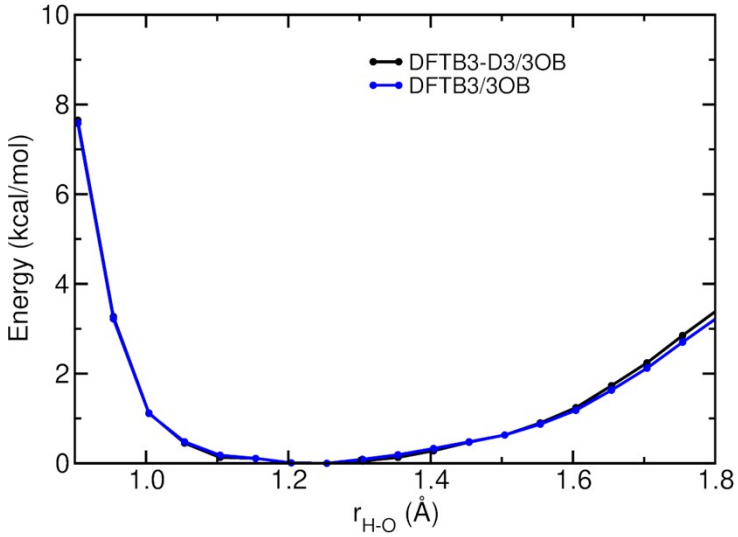

Fig. S16 Energy profile for proton transfer between two BQ radical anions computed using DFTB3/3OB with and without dispersion correction. At distances less than 1.6 Å, the blue and black curves overlap to a large extent.

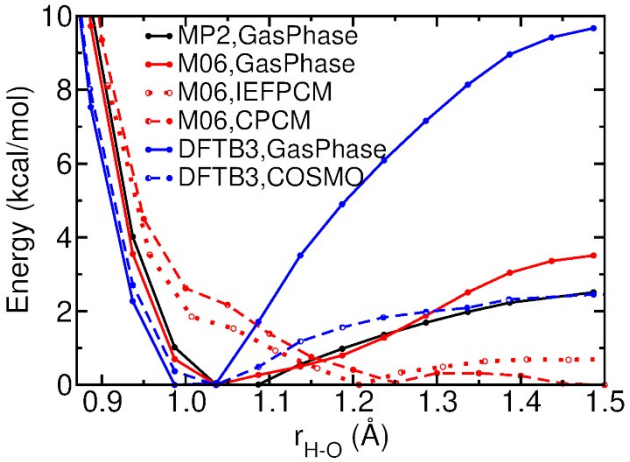

Fig. S17 Energy profile for proton transfer between a neutral PTO molecule and a hydronium ion computed using different methods: MP2/aug-cc-pVDZ in the gas phase, M06/6-31++G** in the gas phase and in implicit solvent described using IEFPCM and CPCM, and DFTB3/3OB in the gas phase and in implicit solvent described using COSMO.

Table S4 Effect of inclusion of solvent on the barrier for PT between two neutral BQ molecules with the donor O-acceptor O distance fixed at 3.52 Å[a]

Method	PT barrier (kcal/mol)
M06[b]	50.4
M06/IEFPCM[b]	53.0
M06/CPCM[b]	53.2
DFTB3/3OB	42.8
DFTB3/3OB/COSMO	44.2

[a]The shape of the PT energy profile remains the same after the inclusion of implicit solvent.
[b]M06 calculations were carried out with the 6-31++G** basis set.

6. Band Structure Calculations

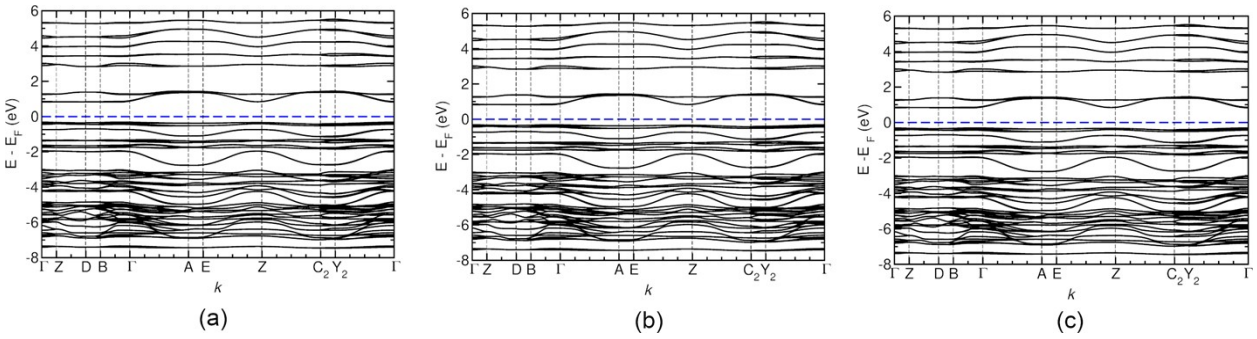

Fig. S18 Band structure for crystalline PTO calculated using PBE-D3 and (a) the optimized norm-conserving (ONCV) pseudopotential, (b) the ultra-soft pseudopotential and (c) the projector augmented wave method. The Fermi level (E_F) is highlighted in blue for easy visualization.

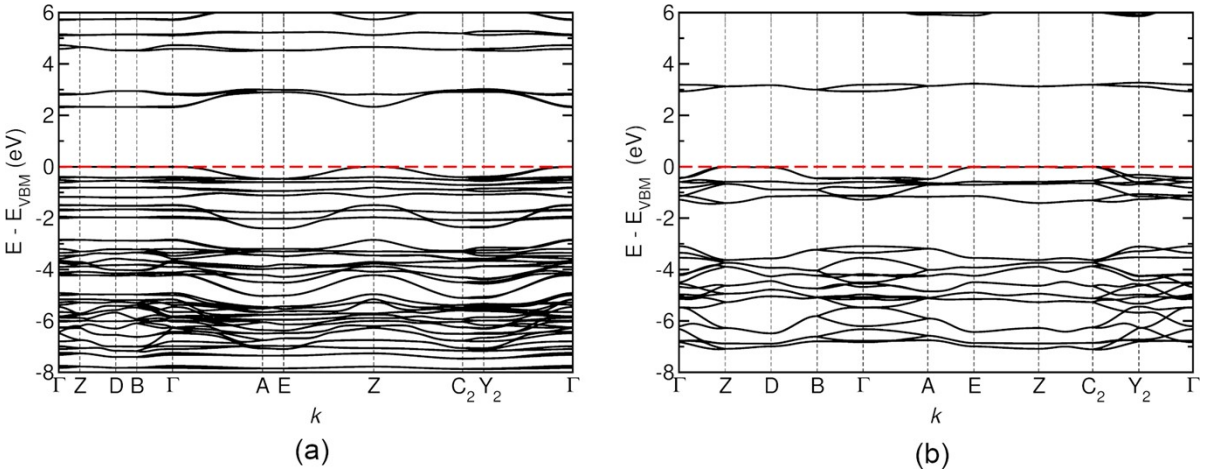

Fig. S19 Band structure for crystalline (a) PTO and (b) BQ calculated using the HSE06 functional and the ONCV pseudopotential. The valence band maximum (E_{VBM}) is highlighted in red for easy visualization.

7. Coordinates of Optimized Geometries

Coordinates of optimized geometries of the molecules and crystals studied have been deposited in a Google Drive repository.

https://drive.google.com/drive/folders/12-wg2x6_WjIlYtMm8-rehIw6c86sQyZd?usp=sharing

References

1. T. Darden, D. York and L. Pedersen, *J. Chem. Phys.*, 1993, **98**, 10089.
2. T. J. Ypma, *SIAM Rev.*, 1995, **37**, 531-551.
3. W. F. V. Gunsteren and H. J. C. Berendsen, *Mol. Simul.*, 1987, **1**, 173-185.
4. J.-P. Ryckaert, G. Ciccotti and H. J. C. Berendsen, *J. Comput. Phys.*, 1977, **23**, 327-341.
5. A. Grossfield, P. N. Patrone, D. R. Roe, A. J. Schultz, D. W. Siderius and D. M. Zuckerman, *Living J. Comp. Mol. Sci.*, 2018, **1**.
6. http://realerthinks.com/block-averaging-bootstrapping-estimating-mean-autocorrelated-data/, (accessed 10/14/2021, 2021).